JOURNAL OF MATERIALS SCIENCE 25 (1990) 4873–4879

X-ray measurements and the structure of polyacrylonitrile- and pitch-based carbon fibres

A. TAKAKU, M. SHIOYA
Department of Organic and Polymeric Materials, Tokyo Institute of Technology, O-okayama, Meguro-ku, Tokyo, Japan

X-ray measurements were carried out on polyacrylonitrile- and pitch-based carbon fibres. The crystallites, disordered regions and microvoids in these carbon fibres were evaluated quantitatively by applying the methods previously proposed by the present authors. The structural parameters evaluated are the 1 1 plane spacing of the carbon layer, the average, standard deviation and asymmetry of the distribution of interlayer spacing, the stacking regularity parallel to the layer plane, the layer extents parallel and perpendicular to the fibre axis, the stacking height, the crystallite orientation, the volume fractions of crystallites, disordered regions and microvoids, the variation of the electron density in a microvoid, and the size parameters of the void cross-section perpendicular to the fibre axis, such as the area, radius of gyration, chord length and thickness. The mutual relationships of these structural parameters are presented, and parameters sensitive to the nature of the starting materials are pointed out.

1. Introduction

As the major structural components of carbon fibres, the following three components may be listed: the crystallite comprising a parallel stacking of carbon layers with a considerable stacking disorder parallel to the layer plane; the microvoid of needle-like shape; and the disordered region in which carbon layers are not associated in the stacking. The presence of these components is evinced, respectively, by the diffuseness or absence of the $h\,k\,l\,(l \neq 0)$ reflections in wide-angle X-ray diffraction (WAXD) patterns [1–3], the strong equatorial streaks in small-angle X-ray scattering (SAXS) patterns [1–5], and the fringes of unorganized carbon layers revealed by transmission electron microscopy [6, 7]. Carbon fibres occasionally contain large flaws at the optical microscopic level [8–11].

Franklin [12] reported that the majority of carbons correspond to one of two well-defined different types: the graphitizing and non-graphitizing carbons. The difference between these two types of carbon is due to the structure of the starting materials. The materials which develop a certain portion of three-dimensionally ordered stacks by heat-treatment at a high temperature should fulfil two essential conditions; that is, in the materials yielding at an early stage of the carbonization process at relatively low temperature, the cross-linking uniting the crystallites is weak, and neighbouring crystallites have a strong tendency to lie in near-parallel orientation. According to Fischer and Ruland [13], the increase in the three-dimensional order of the crystallites has an unfavourable effect on the mechanical properties of the carbon fibres, because it reduces the contribution of the mechanical strength of carbon layers to the macroscopic mechanical properties.

In providing carbon fibres with superior mechanical properties, various processing conditions are certainly as important as the starting material. It is worthwhile to recognize, as a general rule, which structural parameters of carbon fibres are starting material sensitive, and which of those are processing condition sensitive.

In carbon fibres, the layer plane of the crystallites and the longitudinal axis of the microvoids have a strong tendency to orient nearly parallel to the fibre axis. In order to characterize the anisotropic structure of carbon fibres by WAXD and SAXS, X-ray measurements should be carried out on a unidirectionally aligned fibre bundle. It is inappropriate, however, to analyse the X-ray data from a carbon fibre bundle by Bragg's, Scherrer's or Warren's [14] equation or by the theories currently applied to the SAXS of isotropic bodies [15].

This paper reports the results of characterization of the crystallites and microvoids in carbon fibres from two different types of starting materials; polyacrylonitrile (PAN) and pitch. In this work methods developed previously by the present authors for characterizing the crystallites and microvoids in carbon fibres by X-ray measurements on a fibre bundle have been applied [16–20].

2. Materials and methods

2.1. Materials

PAN- and pitch-based carbon fibres covering a wide range of crystallite sizes were collected from commercial sources and supplied for measurements. These fibres were in the form of tow, composed of 2000 to 12 000 filaments varying between types. In addition to these fibres, experimental carbon fibres prepared by pyrolysing petroleum-pitch fibres at temperatures from 1200 to 2600° C with a batch furnace were supplied for measurements.

0022–2461/90 $03.00 + .12

2.2. Measurements

The specimens for X-ray measurements were prepared by forming about 20 000 parallel filaments of carbon fibres into a bundle of rectangular cross-section with a matched die and a small amount of adhesive.

For WAXD and SAXS measurements, a Rigaku-denki diffractometer was used.

The WAXD measurements for all specimens were made under identical diffraction conditions using nickel-filtered CuKα radiation. The detection of the equatorial 0 0 2, 0 0 4, 1 1 and 1 1 2 reflections, the meridional 1 1 reflection and the 0 0 2 diffraction arc was made with a proportional counter by the symmetrical transmission method. For several weak reflections a position-sensitive proportional counter (PSPC) was used, which was set in such a way as to realize the symmetrical transmission at the centre of the angles to be measured. The X-ray absorption of a specimen, in the direction perpendicular to the specimen surface, was determined as the ratio of a strong crystalline reflection intensity measured with and without setting the specimen in the reflected beam.

The SAXS measurements were made on the same specimens used for the WAXD measurements. The incident beam of Cu$K\alpha$ radiation was collimated by two pin-holes of 0.3 and 0.5 mm diameter. The sample-to-detector distance was 360 mm. The equatorial scattering intensity as a function of distance, x, from the centre line of the incident beam was measured using a PSPC with a pulse-height discriminator. No height-limiting slit was attached to the PSPC. Thus, the observed intensity, $I(x)$, can be regarded as the total scattering intensity counted parallel to the fibre axis. The incident X-ray beam flux was determined by measuring the air scattering [16].

The density of carbon fibres was measured at 25° C by a sink–float method using mixtures of carbon tetrachloride, ethylene dibromide, and methylene iodine in case of need.

3. Analysis

3.1. Wide-angle X-ray diffraction

The crystallites in carbon fibres were characterized from WAXD using the following structural parameters: d_{11}, 1 1 plane spacing of the carbon layer; $c/2$, the mean interlayer spacing; σ_c, the standard deviation of the interlayer spacing; τ_c, the asymmetry of the distribution of the interlayer spacing; R, the stacking regularity parallel to the layer plane; $L_{a\parallel}$, the layer extent parallel to the fibre axis; $L_{a\perp}$, the layer extent perpendicular to the fibre axis; L_c, the stacking height; f, the orientation parameter of the crystallites; v_c, the volume fraction of crystallites.

The diffraction angle is represented by 2θ, the angle between the fibre axis and the plane including the incident and diffracted X-rays by ψ, and the WAXD intensities as functions of 2θ and ψ after subtracting the background by I and I', respectively. The diffraction parameters which are determined from the distributions of I and I' for calculating the structural parameters are: $2\theta_p$, the peak diffraction angle; $2\theta_l$, the diffraction angle at half-maximum intensity on the lower angle side of the peak; $2\theta_h$, the diffraction angle at half-maximum intensity on the higher angle side of the peak; $\Delta\psi$, the difference in ψ values at half-maximum intensity of I'; H_{hkl}, the peak intensity of an equatorial $h\,k\,l$ reflection on the intensity distribution, I, which is not separated into respective reflections.

By considering the experimental conditions adopted in this study, the structural parameters may be calculated as follows [18–20].

The parameters $c/2$, σ_c, τ_c and L_c are determined from the equatorial 0 0 2 and 0 0 4 reflections by the equations

$$\frac{\lambda l}{2 \sin \theta_p} = c - \frac{4\pi^2 \tau_c^3 \sigma_c^3}{3c^2} l^2 \quad (1)$$

and

$$\frac{\pi}{\lambda^2 \ln 2} [\sin \theta_h - \sin \theta_l]^2 = \frac{1}{L_c^2} + \frac{4\pi^4 \sigma_c^4}{c^6} l^4 \quad (2)$$

where λ is the X-ray wavelength, and l the reflection index.

The layer extents $L_{a\parallel}$ and $L_{a\perp}$ are determined, respectively, from the meridional and equatorial 1 1 (or 1 1 0) reflections using the equation

$$L_{a\parallel},\ L_{a\perp} = 0.26\lambda/(\sin \theta_p - \sin \theta_l) \quad (3)$$

The orientation parameter, f, is determined from the 0 0 2 diffraction arc by the equation

$$f = 1 - \Delta\psi/\pi \quad (4)$$

The stacking regularity, R, is determined by a trial-and-error method by using the equation

$$\begin{aligned} H_{112} = {} & H_{110} I_{11}(2\theta_{112})/I_{11}(2\theta_{110}) \\ & + [H_{006} - H_{110} I_{11}(2\theta_{006})/I_{11}(2\theta_{110})] \\ & \times [I_{006}(2\theta_{112})/I_{006}(2\theta_{006})] \end{aligned} \quad (5)$$

where $I_{11}(2\theta)$ and $I_{006}(2\theta)$ are the theoretical intensity distributions of the equatorial 1 1 l and 0 0 6 reflections, respectively, and $2\theta_{hkl}$ the $h\,k\,l$ peak diffraction angle in these theoretical intensity distributions [18, 19]. The right-hand side of Equation 5 is a function of R. Therefore, R can be determined by calculating the right-hand side of Equation 5 for various values of R and finding a proper value of R which satisfies Equation 5.

The 1 1 plane spacing d_{11} is determined from the meridional 1 1 reflection by the equation

$$d_{hk} = \lambda/[2 \sin (\theta_p - \delta\theta)] \quad (6)$$

where $\delta\theta$ is a correction factor calculated by simulating the intensity distribution [18, 19].

The crystallite fraction, v_c, can be evaluated from the 0 0 2 reflection by the equation

$$\begin{aligned} v_c = {} & K v_0^2 \sin^2\theta_p \cos \theta_p \int I(2\theta) \mathrm{d}(2\theta) \int I'(\psi) \mathrm{d}\psi / \\ & [t r_s I_e J_a J_s I'(\pi/2)] \end{aligned} \quad (7)$$

where K is a constant, v_0 the volume of the parallelepiped having $\boldsymbol{a}$, $\boldsymbol{b}$ and $\boldsymbol{c}$ as adjacent edges, I_e the X-ray scattering intensity of one electron at the diffraction peak, and J_a the square of the atomic scattering factor of carbon at the diffraction peak. t and r_s

are, respectively, the optical length and the X-ray absorption of a specimen at $2\theta = 2\theta_p$, and are calculated from the X-ray absorption in the direction perpendicular to the specimen surface. J_s takes the form

$$J_s = 1 + R^2 + 2R \cos [2\pi(c \sin \theta_p/\lambda - \zeta)] \quad (8)$$

where

$$R = 1 - 8\pi^2(\sigma_c \sin \theta_p/\lambda)^2 \quad (9)$$

and

$$\zeta = (16\pi^2/3)(\tau_c\sigma_c \sin \theta_p/\lambda)^3 \quad (10)$$

In the present study, in order to eliminate from the calculation the constant K and the intensity of the incident X-ray beam, a highly "graphitized" pitch-based carbon fibre of which v_c was evaluated as the ratio of the fibre density and the crystalline density calculated from lattice constants, was selected as a reference sample, and v_c of the sample to be studied was evaluated from the relative value of the right-hand side of Equation 7 for these two samples with the known value of v_c of the reference sample.

3.2. Small-angle X-ray scattering

The microvoids were characterized from SAXS using the following parameters [16, 17]:

S_3, the average cross-sectional area, which is the average area of a void cross-section perpendicular to the fibre axis and including an arbitrary point in the void;

R_3^2, the square of the average radius of gyration, which is the average of the squared radius of gyration of a void cross-section perpendicular to the fibre axis and including an arbitrary point in the void, where the average is taken by weighting the squared radius of gyration with the cross-sectional area;

l_2, the average chord length, which is the average length of a segment delineated by the contours of the void from a straight line perpendicular to the fibre axis and passing through an arbitrary point in the void;

l_3, the average thickness, which is the average length of a segment delineated by the contours of the void from an arbitrary straight line perpendicular to the fibre axis;

v_p, the volume fraction of microvoids.

The S_3 and R_3 values are determined from the intercept and slope of a straight line approximating the plots of $\ln I(x)$ against x^2 at lower scattering angles, by the equation

$$\ln I(x) = -\frac{2\pi^2 R_3^2}{\lambda^2 L^2} x^2 + \ln S_3 + \ln \left[\frac{2\pi}{\lambda^2 L^2} \int_0^\infty I(x)x \, dx \right] \quad (11)$$

where L is the sample-to-detector distance.

l_2 is calculated from the equation

$$l_2 = \frac{\lambda L \int_0^\infty I(x) \, dx}{\pi \int_0^\infty I(x)x \, dx} \quad (12)$$

l_3 is calculated from the slope of a straight line approximating the plots of $I(x)^{-2/3}$ against x^2 at higher scattering angles, from the equation

$$I(x)^{-2/3} = \left[\int_0^\infty I(x)x \, dx \right]^{-2/3} \times \left[\left(\frac{\lambda L}{2\pi l_3} \right)^{4/3} + \left(\frac{2\pi l_3}{\lambda L} \right)^{2/3} x^2 \right] \quad (13)$$

This parameter depends on the variation of the electron density in microvoids as well as the contour size of microvoids.

v_p is obtained from the equation

$$v_p = \frac{2\pi m^2 c'^4}{e^4 \lambda^3 (\Delta\rho)^2 LtAI_i} \int_0^\infty I(x)x \, dx \quad (14)$$

where $\Delta\rho$ is the electron density difference between a microvoid and the surrounding material, t the specimen thickness, AI_i the incident X-ray beam flux, m the electron mass, e the elementary electric charge, and c' the velocity of light.

In order to characterize the variation of the electron density in microvoids of carbon fibres, the values of ε were calculated. This parameter is defined as

$$\varepsilon = \Delta\rho_p/\langle\Delta\rho\rangle \quad (15)$$

where $\Delta\rho_p$ is the difference between the electron density at the periphery of the microvoids and that of the surrounding material, and $\langle\Delta\rho\rangle$ is the root-mean-square of the electron density difference between the microvoids and the surrounding material. ε is calculated using the equation (see Appendix).

$$\varepsilon = \left\{ \frac{\pi S_3 [\Gamma(4/\alpha)]^3}{4l_3^2 [\Gamma(3/\alpha)]^2 \Gamma(6/\alpha)} \right\}^{1/4} \quad (16)$$

where Γ is a Gamma function, and α a parameter satisfying the equation

$$S_3/R_3^2 = 2\pi \, [\Gamma(6/\alpha)]^2/[\Gamma(4/\alpha)\Gamma(8/\alpha)] \quad (17)$$

If the electron density in a microvoid is even, $\varepsilon = 1$, and if the electron density in the inner part of a microvoid is larger than that at the periphery of the microvoid, $\varepsilon > 1$.

The experimentally observed SAXS intensity distributions were used for analysis after making corrections for air scattering and the X-ray absorption by the specimen and air. The intensity distributions at quite low and quite high scattering angles, which are difficult to measure but are required for carrying out integrations of Equations 11 to 14, were obtained by extrapolating linearly the $(x^2, \ln I(x))$ plot to $x \to 0$ and the $(x^2, I(x)^{-2/3})$ plot to $x \to \infty$.

4. Results and discussion

4.1. Crystallites

4.1.1. Stacking height and heat-treatment temperature

According to the experimental results for a series of pitch-based carbon fibres and the data reported in the literature [3, 13, 21, 22], the stacking height, L_c, as a function of heat-treatment temperature is shown in Fig. 1. The relationships between stacking height and heat-treatment temperature can be categorized into two groups according to the base materials; pitch and PAN. The pitch-based carbon fibres are more

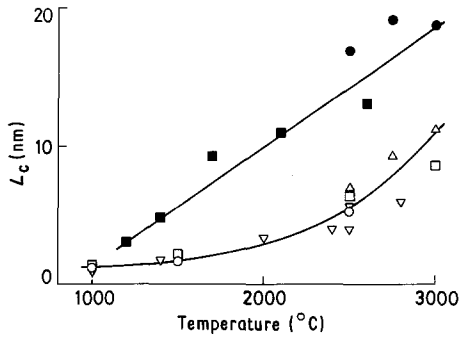

Figure 1 Plots of stacking height, L_c, against heat-treatment temperature for pitch-based carbon fibres (■) present work, (●) Fischer and Ruland [13] and for PAN-based carbon fibres (○) Johnson [3], (△) Fischer and Ruland [13], (▽) Johnson [22], (□) Watt and Johnson [21].

"graphitizable" and give a larger stacking height than the PAN-based carbon fibres at a constant heat-treatment temperature. The stacking height of the pitch-based carbon fibres increases linearly with increasing heat-treatment temperature. With the PAN-based carbon fibres, the growth in stacking height is dominant at temperatures above 2200 to 2500° C.

4.1.2. Lattice spacings

In Figs 2a and b, the 1 1 plane spacing, d_{11}, and the mean interlayer spacing, $c/2$, are represented as functions of the stacking height. The 1 1 plane spacing shows independently of the stacking height, a constant value close to the 1 1 plane spacing of graphite, 0.123 nm. It appears that the layers comprising the crystallites in carbon fibres are nearly the same as those in graphite from an early stage of carbonization which yields a smaller stacking height. The mean interlayer spacing shows a large value of 0.355 nm at smaller stacking heights. It decreases with increasing stacking height, and approaches the value 0.335 nm of graphite.

4.1.3. Stacking regularity

The asymmetry, τ_c, and the standard deviation, σ_c, of the distribution of interlayer spacing, and the stacking

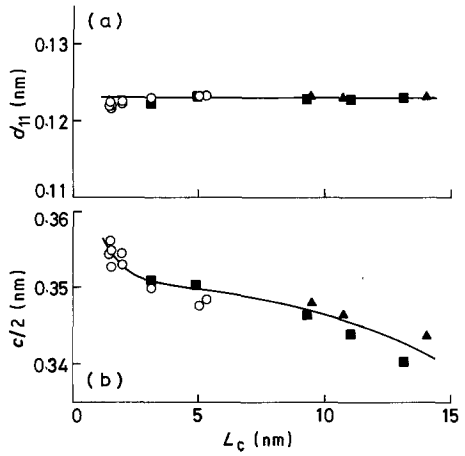

Figure 2 (a) 1 1 plane spacing, d_{11}, and (b) mean interlayer spacing, $c/2$, plotted against stacking height, L_c, for (○) commercial PAN-based, (▲) commercial pitch-based and (■) experimental pitch-based carbon fibres.

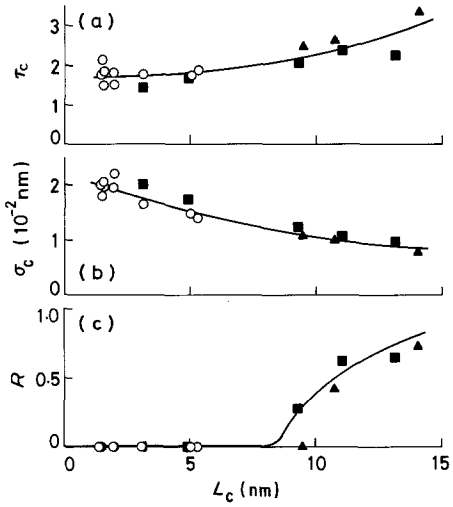

Figure 3 (a) Degree of asymmetry, τ_c, and (b) standard deviation, σ_c, of the distribution of interlayer spacing, and (c) stacking regularity, R, parallel to the layer plane plotted against stacking height, L_c, for (○) commercial PAN-based, (▲) commercial pitch-based and (■) experimental pitch-based carbon fibres.

regularity parallel to the layer plane, R, are plotted against the stacking height in Figs 3a, b and c, respectively. In Figs 4a, b and c, the values of τ_c, σ_c and R are replotted against the mean interlayer spacing.

Values of τ_c are positive for all the carbon fibres studied. A positive value of τ_c implies that the interlayer spacing shows a skewed distribution having a longer tail at larger interlayer spacings [19, 20]. The τ_c value tends to increase with decreasing interlayer spacing, i.e. the distribution of interlayer spacing becomes more asymmetric when the turbostratic carbon structure approaches the graphite structure.

σ_c gradually decreases as the mean interlayer spacing decreases, and is expected to be zero at the mean interlayer spacing of graphite.

R increases at interlayer spacings smaller than about 0.347 nm, and is expected to be unity at the interlayer spacing of graphite; R at spacings larger than 0.347 nm is zero. This indicates that the stacking

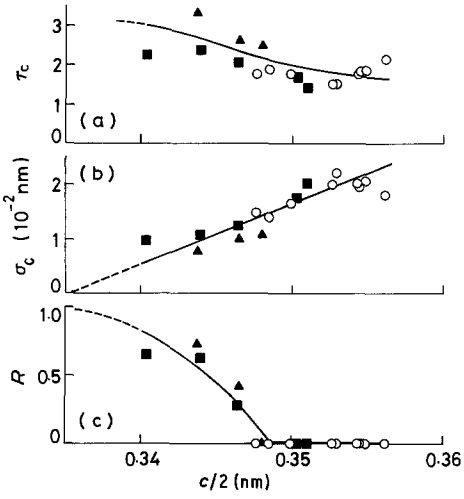

Figure 4 (a) Degree of asymmetry, τ_c, and (b) standard deviation, σ_c, of the distribution of interlayer spacing, and (c) stacking regularity, R, parallel to the layer plane plotted against mean interlayer spacing, $c/2$, for (○) commercial PAN-based, (▲) commercial pitch-based and (■) experimental pitch-based carbon fibres.

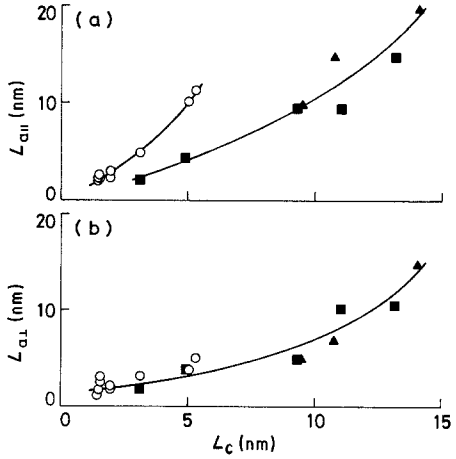

Figure 5 (a) Layer extent parallel to the fibre axis, $L_{a\parallel}$, and (b) layer extent perpendicular to the fibre axis, $L_{a\perp}$, plotted against stacking height L_c for (○) commercial PAN-based, (▲) commercial pitch-based, and (■) experimental pitch-based carbon fibres.

regularity parallel to the layer plane for the carbon fibres showing spacings smaller than about 0.347 nm is almost random. The PAN-based carbon fibres which have been processed even at the highest temperature in this study belong to this category.

4.1.4. Layer extent

The layer extent parallel to the fibre axis, $L_{a\parallel}$, and that perpendicular to the fibre axis, $L_{a\perp}$, are plotted against the stacking height in Figs 5a and b. The $L_{a\parallel}$ value of the PAN-based carbon fibres is larger than that of the pitch-based carbon fibres at a constant stacking height. In contrast, there is no obvious difference due to the starting materials in the relation between $L_{a\perp}$ and stacking height.

It is stated that the layer stacking in PAN-based carbon fibres can grow in the orientation direction of the original PAN molecular axis, but is difficult to grow perpendicular to this direction.

4.1.5. Orientation

The orientation parameter, f, is plotted against the layer extent $L_{a\parallel}$ in Fig. 6. A good correlation is found between these structural parameters.

Fourdeux *et al.* [2] have proposed a "ribbon-like model" for the structure of carbon fibres, in which ribbon-like carbon layers are stacked side by side, and are slowly undulating along the direction of the fibre

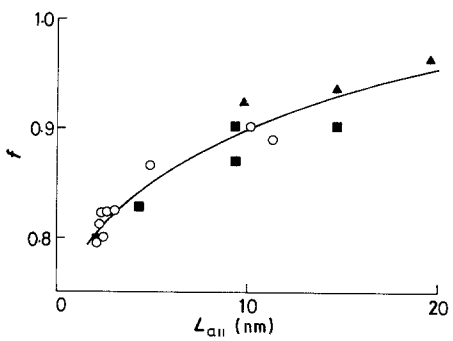

Figure 6 Orientation parameter, f, plotted against layer extent parallel to the fibre axis, $L_{a\parallel}$, for (○) commercial PAN-based, (▲) commercial pitch-based and (■) experimental pitch-based carbon fibres.

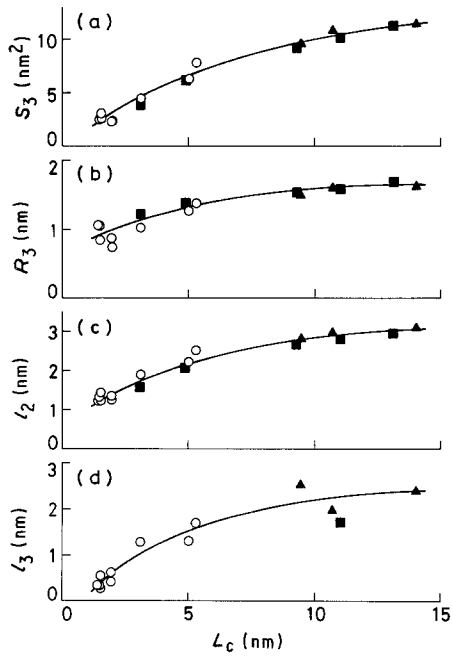

Figure 7 Size parameters characterizing void cross-section perpendicular to the fibre axis: (a) average area S_3; (b) average radius of gyration R_3, (c) average length l_2, and (d) average thickness l_3, plotted against stacking height L_c for (○) commercial PAN-based [17], (▲) commercial pitch-based and (■) experimental pitch-based carbon fibres.

axis. The layer extent, $L_{a\parallel}$, is regarded as the length of the straight portions of the undulating carbon layer stacks. The result in Fig. 6 shows that an increase in length of the straight portions of the undulating stacks leads to an increase in the orientation of the stacks.

4.2. Microvoids

The size parameters of void cross-section perpendicular to the fibre axis, S_3, R_3, l_2 and l_3, are shown as functions of the stacking height in Figs 7a, b, c and d, respectively. The SAXS for pitch-based carbon fibres of some types was so weak that l_3 could not be determined with sufficient accuracy.

The size parameters S_3, R_3 and l_2 are insensitive to the electron density distribution in the microvoids. The plots of these parameters can be approximated by single curves. This indicates that the contour size of the void cross-section perpendicular to the fibre axis is determined in association with the growth of the stacking height, independent of the kinds of starting materials.

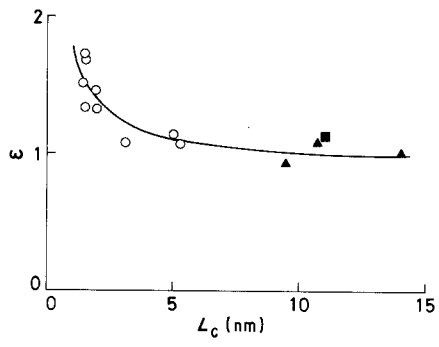

Figure 8 Variation in electron density, ε, plotted against stacking height, L_c, for (○) commercial PAN-based, (▲) commercial pitch-based and (■) experimental pitch-based carbon fibres.

ε is plotted against the stacking height in Fig. 8. ε decreases with increasing stacking height in a unique fashion, independent of the types of starting materials, and approaches unity at a stacking height of about 8 nm.

4.3. Volume fractions of structural components

The density–stacking height relation is quite different between the PAN- and pitch-based carbon fibres as shown in Fig. 9, and the densities for the PAN-based carbon fibres are generally lower than those for the pitch-based carbon fibres.

The crystallite fraction, v_c, and the microvoid fraction, v_p, can be evaluated, respectively, from Equations 7 and 14. By assuming that the structure of carbon fibres is composed of three components, i.e. crystallites, unorganized carbons and microvoids, and that the sum of the fractions of these three structural components is unity, the volume fraction of unorganized carbons can be calculated. The results of the calculation are shown in Figs 10a to c as functions of the stacking height, where the values of v_p were evaluated, by assuming that the microvoids are of vacant space, from Equation 14 with values of $\Delta\rho$ calculated from the fibre densities.

It is noted in Fig. 10 that the fraction v_c for carbon fibres of various origins exhibits a similar dependence on the stacking height, but that the fractions v_a and v_p do not. At a constant stacking height, the PAN-based carbon fibres contain a larger fraction of microvoids and a smaller fraction of unorganized carbons than the pitch-based carbon fibres.

5. Conclusions

1. At a constant heat-treatment temperature, the stacking height of PAN-based carbon fibres gives a smaller value than that of pitch-based carbon fibres. The unit cell of the individual carbon layers in the crystallites of carbon fibres prepared with different conditions from various starting materials are almost the same in dimensions as that of graphite.

2. The distribution asymmetry of interlayer spacing and the extent of stacking regularity increase as the interlayer spacing approaches the value of graphite. The stacking regularity parallel to the layer plane is almost random at mean interlayer spacings larger than about 0.347 nm.

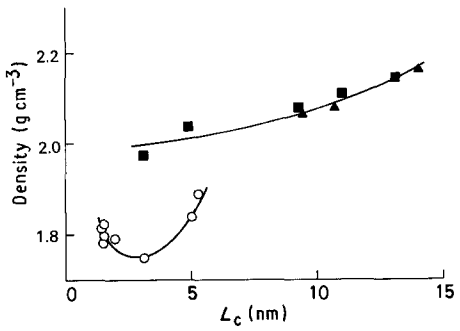

Figure 9 Fibre density plotted against stacking height, L_c, for (○) commercial PAN-based [17], (▲) commercial pitch-based and (■) experimental pitch-based carbon fibres.

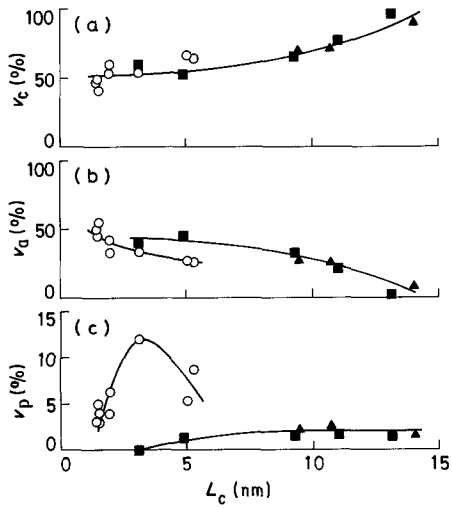

Figure 10 Volume fraction of (a) crystallites, v_c, (b) that of unorganized carbons, v_a, and (c) that of microvoids, v_p plotted against stacking height L_c for (○) commercial PAN-based, (▲) commercial pitch-based and (■) experimental pitch-based carbon fibres.

3. The layer extent perpendicular to the fibre axis, the volume fraction of crystallites, the size and internal electron density distribution of microvoids vary cooperatively with the growth of the stacking height.

4. The layer extent parallel to the fibre axis, the fractions of unorganized carbon and microvoids are sensitive to the types of starting material. A correlation is found between the crystalline orientation and the layer extent parallel to the fibre axis.

Appendix

Assume that the electron density in the microvoids is constant and that the cross-sections of the microvoids, perpendicular to the fibre axis, are of circular shape with radius r which distributes according to a probability density function

$$f(r) = \frac{\alpha}{\Gamma(2/\alpha)r_0}\left(\frac{r}{r_0}\right)\exp\left[-\left(\frac{r}{r_0}\right)^{\alpha}\right] \quad \text{(A1)}$$

The parameters S_3, R_3, l_2 and l_3 are then given by

$$S_3 = \pi r_0^2\Gamma(6/\alpha)/\Gamma(4/\alpha) \quad \text{(A2)}$$

$$R_3^2 = (r_0^2/2)\Gamma(8/\alpha)/\Gamma(6/\alpha) \quad \text{(A3)}$$

$$l_2 = [16r_0/(3\pi)]\Gamma(5/\alpha)/\Gamma(4/\alpha) \quad \text{(A4)}$$

and

$$l_3 = (\pi r_0/2)\Gamma(4/\alpha)/\Gamma(3/\alpha) \quad \text{(A5)}$$

α and r_0 can be calculated from the observed values of S_3 and R_3 using Equations A2 and A3. Then, the values of l_2 and l_3 can be calculated according to Equations A4 and A5. For various types of carbon fibres, the calculated values of l_2 agree quite well with the observed values. A calculated value of l_3, which is denoted l_3', however, shows a larger value than that observed [17]. Because the parameters S_3, R_3 and l_2 are insensitive to the electron density at the periphery of the microvoids, l_3' reflects the size and shape of the contour of the microvoids. The discrepancy between the values of l_3 and l_3', therefore, is caused by the

variation in the electron density at the periphery of the microvoids.

Let us divide the microvoids into infinitely thin sections perpendicular to the fibre axis and designate the electron density of the kth section as $\Delta\rho_k(\boldsymbol{x})$. Then, l_3 is represented by [16, 17]

$$l_3 = \left[-\lim_{a\to 0} \frac{\mathrm{d}}{\mathrm{d}a} \times \frac{\sum_k \int \Delta\rho_k(\boldsymbol{x})\Delta\rho_k(x_1 - a, x_2, x_3)\,\mathrm{d}v_x}{\sum_k \int [\Delta\rho_k(\boldsymbol{x})]^2\,\mathrm{d}v_x} \right]^{-1} \quad \text{(A6)}$$

where x_3 is the component of the real-space vector $\boldsymbol{x}$ in the direction parallel to the fibre axis, and $\mathrm{d}v_x$ the volume element. Thus, independent of the shape and size distribution of the microvoid cross-section, we have

$$l_3'/l_3 = [\Delta\rho_p/\langle\Delta\rho\rangle]^2 \quad \text{(A7)}$$

From Equations 15, A2, A3, A5 and A7, Equations 16 and 17 are obtained. A value of ε obtained by assuming that the cross-sections of the microvoids, perpendicular to the fibre axis, are of elliptical shape [17] gives almost the same value as that calculated using Equation 16.

References

1. R. PERRET and W. RULAND, *J. Appl. Cryst.* **3** (1970) 525.
2. A. FOURDEUX, R. PERRET and W. RULAND, in "International Conference on Carbon Fibres – their Composites and Applications", Paper no. 9 (The Plastics Institute, London, 1971).
3. D. J. JOHNSON, *Phil. Trans. R. Soc. Lond.* **A294** (1980) 443.
4. D. J. JOHNSON and C. N. TYSON, *J. Phys. D* **2** (1969) 787.
5. *Idem, ibid.* **3** (1970) 526.
6. D. CRAWFORD and H. MARSH, *J. Microscopy* **109** (1) (1977) 145.
7. M. GUIGON, A. OBERLIN and G. DESARMOT, *Fibre Sci. Technol.* **20** (1984) 55.
8. J. W. JOHNSON, *Appl. Polym. Symp.* **9** (1969) 229.
9. J. V. SHARP and S. G. BURNAY, in "International Conference on Carbon Fibres – their Composites and Applications", Paper no. 10 (The Plastics Institute, London, 1971).
10. S. CHWASTIAK, J. B. BARR and R. DIDCHENKO, *Carbon* **17** (1979) 49.
11. S. C. BENNETT, D. J. JOHNSON and W. JOHNSON, *J. Mater. Sci.* **18** (1983) 3337.
12. R. E. FRANKLIN, *Proc. Roy. Soc. Lond.* **A209** (1951) 196.
13. L. FISCHER and W. RULAND, *Colloid Polym. Sci.* **258** (1980) 917.
14. B. E. WARREN, *Phys. Rev.* **59** (1941) 693.
15. A. GUINIER and G. FOURNET, "Small-angle scattering of X-rays" (Wiley, New York, 1955).
16. M. SHIOYA and A. TAKAKU, *J. Appl. Phys.* **58** (1985) 4074.
17. A. TAKAKU and M. SHIOYA, *J. Mater. Sci.* **21** (1986) 4443.
18. M. SHIOYA and A. TAKAKU, *Acta Crystallogr.* **A44** (1988) 150.
19. *Idem, J. Appl. Crystallogr.* **22** (1989) 222.
20. *Idem, Carbon,* **28** (1990) 165.
21. W. WATT and W. JOHNSON, *Appl. Polym. Symp.* **9** (1969) 215.
22. D. J. JOHNSON, in "International Conference on Carbon Fibres – their Composites and Applications", Paper no. 8 (The Plastics Institute, London, 1971).

Received 26 June
and accepted 1 December 1989